JOURNAL OF PROPULSION AND POWER
Vol. 25, No. 1, January–February 2009

Diffusion Flame Calculations for Composite Propellants Using a Vorticity-Velocity Formulation

Matthew L. Gross* and Merrill W. Beckstead†
Brigham Young University, Provo, Utah 84602

DOI: 10.2514/1.36360

A two-dimensional model has been developed to study the flame structure above composite propellants using a vorticity-velocity formulation of the transport equations. This formulation allows for a more stable, robust, accurate, and faster solution method compared with the compressible Navier–Stokes equations in the low Mach flow regime. The model includes mass and energy coupling between the condensed and gas phases. The condensed-phase model is based on previously reported one-dimensional models and includes distributed decomposition and multistep-reaction kinetics. The model uses a detailed gas-phase kinetic mechanism consisting of 37 species and 127 reactions. The kinetic mechanism and species diffusion determine the flame structure of the system; no assumptions are made beforehand, aside from appropriate boundary conditions. Numerical studies have been performed to examine the flame structure above an ammonium-perchlorate/hydroxy-terminated-polybutadiene propellant. The predicted flame structure was found to be qualitatively similar to the Beckstead-Derr-Price model with both premixed and diffusion flames present. Results present significant insight into ammonium perchlorate's ability to control a propellant's burning rate and illustrate the importance of the primary diffusion flame in composite propellant combustion.

Nomenclature

c_p	=	heat capacity, erg/g/K
$\mathbf{g}$	=	gravitational acceleration vector, cm/s^2
h	=	specific enthalpy, erg/g
i	=	species index
M	=	Mach number
r	=	radial distance, cm
r	=	radial direction
T	=	temperature, K
t	=	time, s
$\mathbf{v}$	=	velocity vector, cm/s
$\hat{v}$	=	diffusion velocity, cm/s
W	=	molecular mass, g/mol
$\dot{w}$	=	chemical production rate, g/cm^3/s
Y	=	mass fraction
z	=	axial direction
λ	=	thermal conductivity, erg/s/cm/K
μ	=	viscosity, poise
ρ	=	density, g/cm^3
Φ	=	dissipation function
$\boldsymbol{\omega}$	=	vorticity vector, 1/s

I. Introduction

AMMONIUM perchlorate (AP) has been in use as a major propellant ingredient for decades. AP is the standard ingredient in solid rocket propellants and is used in many applications: ballistic missiles, military attack missiles, space applications, etc. Two major reasons for AP's widespread use are its stability, resulting in safe munitions, and its ability to control a propellant's burning rate. By varying the AP particle-size distribution, it is possible to achieve vastly different overall propellant burning rates. No other current oxidizer has the capacity to control a propellant's burning rate in this manner. This unique behavior of AP has not been accurately predicted using detailed a priori numerical models; thus, empirical studies are still relied upon heavily to characterize AP-containing propellants.

Combustion of solid propellants involves a combination of processes evolving from the various ingredients that constitute the propellant. These ingredients decompose, evaporate, and/or pyrolyze, giving off gases, which then react, resulting in energetic flames that drive the combustion process of the propellant. Based on the oxidizer size and type, these energetic flames may be premixed, diffusion, or a combination of both. The combustion of AP composite propellants is dominated by the diffusional processes, resulting in the characteristic particle-size dependence of composite propellants. In other (non-AP-containing) propellants, the effect of the diffusion process appears to be much reduced, relative to AP propellants. Apparently, the chlorine chemistry has a very significant effect on the combustion, which is not observed in other propellants. Unfortunately, the extremely small scale of the particles and flames involved make experimental resolution virtually impossible at any practical pressure. Therefore, there is still some debate as to the exact mechanisms involved in AP composite propellant combustion.

To investigate the impact of diffusion flames on composite propellant combustion, a multidimensional model with detailed chemical kinetics has been developed [1–5]. This two-dimensional model also provides a framework in which detailed kinetic mechanisms can be developed and applied to premixed and diffusion flames above an idealized burning propellant. Work by a number of researchers has focused on the complex surface geometric effects, employing global or semiglobal reactions in the gas phase. The current model instead focuses attention on the complex kinetics of the gas phase. No assumptions have been made as to the flame structure, aside from appropriate boundary conditions. The interaction between diffusional processes and the detailed gas-phase kinetic mechanism is allowed to completely determine the flame structure. This detailed model has been applied to an idealized ammonium-perchlorate/hydroxy-terminated-polybutadiene (AP/HTPB) composite propellant, and calculations show encouraging promise toward simulating the minute detail involved in the combustion process that determines the burning rates of AP-containing propellants.

Received 26 December 2007; accepted for publication 5 September 2008.

*Graduate Student, Chemical Engineering Department, 350 Clyde Building; matthew.gross1@navy.mil.

†Professor, Chemical Engineering Department, 350 Clyde Building; Associate Fellow AIAA.

II. Background

AP has been the subject of numerous experimental and theoretical studies in an attempt to explain its unique properties. The most widely accepted theoretical picture, the Beckstead-Derr-Price (BDP) model, was developed in 1970 [6,7]. The BDP physical picture is presented in Fig. 1. This model proposes that the combustion region above the surface of AP and the corresponding binder/fuel is composed of three competing flames: the primary diffusion flame between the AP decomposition products and the binder decomposition products, the AP monopropellant flame, and the final diffusion flame between the AP monopropellant flame products and the binder products (mixed with the primary diffusion flame products). The impact of these three flames on the propellant burning rate varies with particle size and pressure.

According to the BDP model, large AP particles burn more slowly than small AP particles, being driven primarily by the relatively cool premixed self-deflagrating AP flame above their surface. On the other hand, the decomposition products from very small particles in the binder matrix are able to intimately mix with binder pyrolysis products, resulting in an approximately one-dimensional hot premixed flame over the AP/binder. Combustion of particles of intermediate diameter is driven by a combination of these effects, with hot diffusion flames near the particle edges competing with the AP monopropellant for AP decomposition products. This flame structure provides spatially varying heat feedback to the surface. A previously predicted particle-size dependence of an AP/HTPB propellant's burning rate is illustrated graphically in Fig. 2 [7]. Note that large particles (greater than 200 μm) begin to approach the monopropellant burning rate of AP, whereas a continual decrease in particle size increases the burning rate of the propellant until a premixed limit is reached, at which point the burning rate no longer changes with particle size. The shape of the curve presented in Fig. 2 varies with propellant formulation and pressure.

Numerous numerical models have been developed in an attempt to predict the effects of changing propellant formulation and operating conditions on the complex combustion of composite propellants. These models have progressed through various levels of complexity, from one-dimensional to multidimensional models and from global or semiglobal gas-phase kinetics to detailed reaction mechanisms with dozens of species and hundreds of reactions. The primary diffusion flame is assumed to be a dominant driving force in AP composite propellant combustion leading to the particle-size effect; consequently, it must be considered in any model attempting to describe AP-based propellants. Thus, two-dimensional models have been evolving to describe the diffusion flame structure associated with AP [1,8,9]. The surface boundary conditions for the diffusion flames depend on the sizes of the particles and the distance between particles. Therefore, to effectively accomplish such modeling requires some kind of assumption or calculation of the structure of the propellant surface.

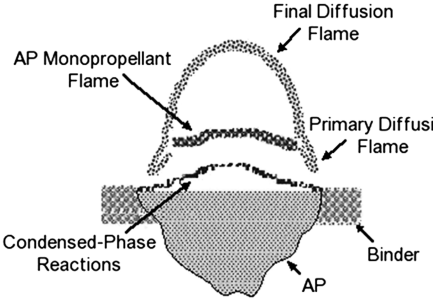

Fig. 1 Proposed BDP flame structure above an AP/HTPB composite propellant.

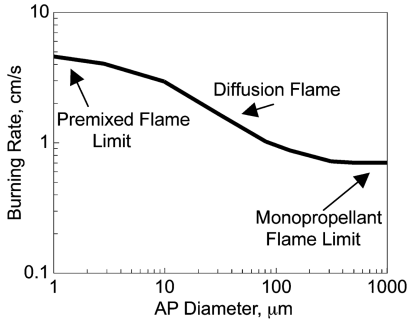

Fig. 2 Predicted particle-size dependence of AP burning rate at 68 atm [7].

Various researchers have recently developed two- and three-dimensional methodologies to describe the geometric packing effects within solid propellants [10–16]. These models have the potential to provide the necessary boundary conditions for the diffusion flame calculations. The earliest of these is the work by Davis and Carter [10] and Webb and Davis [11] on the ParPack code that has been ongoing for some time. Sankaralingam and Chakravarthy [12] also recently developed a packing model to describe composite propellants. Researchers at the University of Illinois at Urbana–Champaign have been very active in this area as well [13–16]. These models represent significant progress toward developing a realistic geometrical packing description of a solid propellant. Unfortunately, a quantitative evaluation of the accuracy of these models is difficult, due to both a lack of quantitative data on the geometrical distribution of particles in the processed propellant and the random nature of actual propellants.

Using these packing models, complex unsteady heat transfer and propellant surface regression for oxidizer/binder sandwiches and 2-D and 3-D random packs of propellant particles have also been modeled, but only using global 2- and 3-step reaction mechanisms to describe the gas-phase heat release. A significant effort has been expended by researchers at the Center for the Simulation of Advanced Rockets, University of Illinois at Urbana–Champaign [17], to model composite propellants. Their initial combustion model assumed a premixed AP flame and a final diffusion flame only, and their initial burning-rate results were poor [17]. They then added a third flame to their combustion model, assuming a three-flame model similar to the BDP model [18], which improved their results.

An alternative to using particle-packing models with global kinetics is to use detailed gas-phase kinetics with simplified geometry. Research by Parr et al. [19,20] used experimental and modeling work to examine AP/hydrocarbon combustion using a counterflow device. The experimental setup consisted of a burning AP pellet with an opposed hydrocarbon stream 5 mm away at 0.92 atm. Flow rates were controlled so that the two gaseous jets met in the middle of the apparatus. Numerical calculations agreed reasonably well with experimental data. However, such an experimental setup eliminates the primary diffusion flame described by the BDP model, and the numerical model's principal focus was the final diffusion flame. Thus, the study helped to verify the far-field kinetics of the final diffusion flame at atmospheric conditions, but did not fully address the premixed AP flame and neglected the primary diffusion flame altogether. Further, the scale and operating pressure make extrapolation to experimental conditions very difficult, although this is the challenge faced by all experimental designs.

The current work also focuses on incorporating realistic kinetics into a two-dimensional detailed numerical diffusion model. However, the focus will be on predicting the flame structure above a propellant's surface based on realistic scales and operating pressures. The work performed at the University of Illinois at Urbana–Champaign focused in great detail on the condensed-phase processes and used a simplified gas phase, whereas the current work focuses on the details of the gas phase and uses a simplified condensed phase. Calculations using the detailed gas-phase mechanism give great insight into the fundamental mechanisms involved in AP/hydrocarbon combustion and illustrate that both kinetics and diffusion steps have to be modeled with appropriate chemistry and physics. Coupling these calculations with a geometric calculation to determine an actual propellant burning rate is yet to be accomplished.

A. Model Modifications

The first iteration of the diffusion flame model, developed by Felt and Beckstead [1] and Felt [2], solved the fully coupled Navier–Stokes conservation equations. Use of these equations results in a tightly coupled, nonlinear system; the system is coupled because multiple dependent variables appear in the same equation, and it is nonlinear because products of the dependent variables appear in the equations [21]. A major difficulty in solving the governing equations results from the tight coupling of pressure and velocity: a small change in pressure results in a large change in velocity. Numerical difficulties become even more prominent at low Mach numbers ($M < 0.3$) using the fully coupled Navier–Stokes equations, due to the pressure term being on the order of $1/M^2$. As the Mach number approaches zero, use of the fully coupled conservation equations begins to suffer in efficiency and accuracy. In spite of these increased numerical difficulties as M approaches zero, pressure is only a weak function of density; therefore, it is of minimal importance [22]. Another numerical difficulty is the hyperbolic characteristic of the momentum equations [21], because of the first-order pressure term, which dictates the use of a time-marching technique to reach a steady-state solution. These hyperbolic characteristics create a very strong convergence dependence on initial conditions. Poor initial conditions result in difficulty obtaining a steady-state solution. Also, the very small scale necessary to resolve the flame dictated time steps between 10^{-8} and 10^{-11} s based on the Courant–Friedrichs–Lewy criteria [23]. The Felt [2] model suffered from efficiency and accuracy problems due to these inherent numerical difficulties. Model calculations would take weeks to converge, dozens of code crashes would be experienced due to divergence, and the final solution could be inaccurate. Therefore, modification of the model to a low Mach number solution technique was undertaken.

Low Mach number formulations essentially filter out the acoustics from the pressure field. A number of methods are available for low Mach flow. Such methods fall into two categories: density-based methods and pressure-based methods [22]. Density-based methods modify the compressible equations to work in the low Mach regime, whereas pressure-based methods extrapolate the corresponding incompressible equations up to the low Mach region. Density-based methods seemed most appropriate in this study because of the reactive nature of the flow. The methods investigated included the SIMPLE method [24], projection methods such as the method used by Massa et al. [25], and the vorticity method used by Smooke et al. [26]. Implementation of the SIMPLE or projection methods required vast changes to the solving technique used in the Felt [2] code. Therefore, the vorticity method was chosen because it could be solved using the Newton–Raphson method.

B. Conservation Equations

A steady-state vorticity-velocity formulation of the conservation equations, based on work by Smooke et al. [26], Bennett and Smooke [27], and Dworkin et al. [28], is solved with appropriate boundary conditions. This method filters the pressure and results in elliptical equations, which can eliminate the need for pseudo-time-stepping to reach a steady-state solution and greatly decrease CPU time. Vorticity represents the angular rotation rate of a fluid and is defined as the curl of the velocity field. Pressure appears in the Navier–Stokes equation in the form of a gradient and, by definition, the curl of a gradient is zero. Therefore, conversion of the Navier–Stokes equations to a vorticity formulation effectively eliminates the pressure-field calculation and takes advantage of the essentially isobaric nature of the system. Vorticity has been employed extensively for incompressible flow calculations. Work by Smooke et al. [26] resulted in the development of a vorticity-stream function formulation for use with compressible two-dimensional diffusion flame calculations. Their work was further refined to a vorticity-velocity formulation [27,28] and is the basis for the vorticity-velocity formulation employed in this study. Equations (1–5) present the two-dimensional equations in cylindrical form [28], including the ideal-gas forms of the energy equation [21] and species continuity equation [29]. Viscous dissipation is included in the energy equation and gravity is included in the vorticity equation for completeness, however, both terms are essentially zero for the small scale and slow velocities of the current problem.

Radial velocity:

$$\frac{\partial^2 v_r}{\partial r^2} + \frac{\partial^2 v_r}{\partial z^2} - \frac{\partial \omega}{\partial z} + \frac{\partial}{\partial r}\left(\frac{v_r}{r}\right) + \frac{\partial}{\partial r}\left(\frac{v_r}{\rho}\frac{\partial \rho}{\partial r} + \frac{v_z}{\rho}\frac{\partial \rho}{\partial z}\right) = 0 \tag{1}$$

Axial velocity:

$$\frac{\partial^2 v_z}{\partial r^2} + \frac{\partial^2 v_z}{\partial z^2} + \frac{\partial \omega}{\partial r} + \frac{1}{r}\frac{\partial v_r}{\partial z} + \frac{\partial}{\partial z}\left(\frac{v_r}{\rho}\frac{\partial \rho}{\partial r} + \frac{v_z}{\rho}\frac{\partial \rho}{\partial z}\right) = 0 \tag{2}$$

Vorticity:

$$\begin{aligned}&\frac{\partial^2(\mu\omega)}{\partial r^2} + \frac{\partial^2(\mu\omega)}{\partial z^2} + \frac{\partial}{\partial r}\left(\frac{\mu\omega}{r}\right) - \rho v_r \frac{\partial \omega}{\partial r} - \rho v_z \frac{\partial \omega}{\partial z} \\ &\quad + \frac{\rho v_r \omega}{r} - \bar{\nabla}\rho \cdot \nabla\left(\frac{\mathbf{v}\cdot\mathbf{v}}{2}\right) + \bar{\nabla}\rho \cdot \mathbf{g} \\ &\quad - 2\left(\bar{\nabla}(\mathrm{div}(\mathbf{v})) \cdot \nabla\mu - \nabla v_r \cdot \bar{\nabla}\frac{\partial \mu}{\partial r} - \nabla v_z \cdot \bar{\nabla}\frac{\partial \mu}{\partial z}\right) = 0\end{aligned} \tag{3}$$

Energy:

$$\begin{aligned}&\rho c_p\left(v_r\frac{\partial T}{\partial r} + v_z\frac{\partial T}{\partial z}\right) - \frac{1}{r}\frac{\partial}{\partial r}\left(r\lambda\frac{\partial T}{\partial r}\right) - \frac{\partial}{\partial z}\left(\lambda\frac{\partial T}{\partial z}\right) \\ &\quad + \rho\sum_{i=1}^{K}\left[c_{p,i}Y_i\left(\hat{v}_{i,r}\frac{\partial T}{\partial r} + \hat{v}_{i,z}\frac{\partial T}{\partial z}\right)\right] + \sum_{i=1}^{K} h_i W_i \dot{w}_i + \Phi = 0\end{aligned} \tag{4}$$

Species continuity:

$$\rho v_r\frac{\partial Y_i}{\partial r} + \rho v_z\frac{\partial Y_i}{\partial z} + \frac{1}{r}\frac{\partial}{\partial r}(r\rho Y_i \hat{v}_{i,r}) + \frac{\partial}{\partial z}(\rho Y_i \hat{v}_{i,z}) - W_i\dot{w}_i = 0 \tag{5}$$

where $\bar{\nabla} = \hat{\mathbf{r}}\partial/\partial z - \hat{\mathbf{z}}\partial/\partial r$ and $\mathrm{div}(\mathbf{v}) = 1/r\partial(rv_r)/\partial r + \partial v_z/\partial z$.

C. Boundary Conditions

The system of equations is closed with appropriate boundary conditions for all sides of the computational domain. The inflow boundary conditions are determined through iteration with the condensed phase. To get meaningful inlet boundary conditions without dynamically modeling the condensed phase, calculations were made using one-dimensional AP [30] and AP/HTPB [31] models. These one-dimensional models solve the coupled gas/condensed-phase problem for each individual ingredient. One-dimensional calculations were performed over a range of compositions from pure AP to 75%-AP/25%-HTPB and a range of pressures. Mass flux, species mass fractions, and surface temperature from these calculations were then correlated with the predicted gas-phase heat flux before running the diffusion flame model. The inlet boundary conditions for the two-dimensional diffusion flame model are then determined by calculating the surface heat flux at each node and feeding these values into the previously determined heat flux correlations. This iterative process is continued until the model converges. Such an approach neglects any two-dimensional effects in the condensed phase, but greatly simplifies the calculation of the dynamic gas-phase inlet boundary conditions (This is the same approach used in the Felt [2] model.) The inflow boundary conditions are presented in Eq. (6):

$$\begin{aligned}&\rho v_z, T, Y_{i\ \mathrm{condensed}} = \text{heat flux correlations} \\ &\omega = \frac{\partial v_r}{\partial z} - \frac{\partial v_z}{\partial r}, \qquad v_r = 0\end{aligned} \tag{6}$$

The particle centerline and outer radial boundary conditions were assumed to be symmetrical with no radial velocity or radial gradients [see Eq. (7)]:

$$v_r = \omega = \frac{\partial v_z}{\partial r} = \frac{\partial T}{\partial r} = \frac{\partial Y_i}{\partial r} = 0 \tag{7}$$

The outflow is treated as a far-field boundary condition, in which the radial velocity vanishes as do axial gradients of the remaining variables [Eq. (8)]:

$$v_r = \frac{\partial \omega}{\partial z} = \frac{\partial v_z}{\partial z} = \frac{\partial T}{\partial z} = \frac{\partial Y_i}{\partial z} = 0 \tag{8}$$

D. Thermodynamics and Transport Properties

Solution of the conservation equations requires the calculation of various multicomponent thermodynamic and transport properties. These properties include density, mean molecular weight, specific heat, enthalpy, chemical reaction rates, viscosity, diffusivity, and thermal conductivity. The CHEMKIN libraries are used to calculate these properties [32,33]. CHEMKIN is a problem-independent, general-purpose suite of software from Sandia National Laboratories, developed in the 1980s. The CHEMKIN libraries standardize the input of chemical properties into numerical models by using a database of thermodynamic and transport properties for individual species. The thermodynamic database includes polynomial fits of specific heat (c_p^o/R), enthalpy (H^o/RT), and entropy (S^o/RT) for each species. The transport database consists of molecule geometry, Lennard-Jones potential well depth, Lennard-Jones collision diameter, dipole moment, polarizability, and rotational relaxation for each species. Input values for the thermodynamic and transport properties were taken from Jeppson [31].

E. Solution Technique

The method of discretization used for the current problem is a form of the control-volume approach based on the work of Patankar [24]. The control-volume method divides the numerical domain into a series of nonoverlapping volumes containing a single point at the center of the volume. The differential equations are then integrated across the control volume. Such a methodology results in the conservation of dependent variables across the control volume and the conservation of fluxes at the cell interface. The current model uses a second-order discretization for the diffusion terms and the first-order upwind method for the convective terms, thus making the overall model first-order-accurate. To help ensure accuracy, both axial and radial velocities are calculated using a staggered grid, and a successive ratio is used to group nodes near the surface and the AP/binder interface.

Once the partial differential equations are approximated, the system of algebraic equations is then solved using an iterative Newton–Raphson method that requires an initial estimate of the solution. When a reasonable initial guess is not possible, a time-marching technique is employed to progress the solution toward convergence. This introduces the stability of a time-marching technique, but without the low Mach flow difficulties inherent in the Navier–Stokes equations. Transient terms are added to the vorticity, energy, and species equations when a time-marching technique is desired, converting the elliptical equations to parabolic equations. Once the solution appears to be within range of the final solution (based on the solver residual) the transient terms are removed and the program rapidly converges. This technique has been used successfully by Bennett and Smooke [27] for the vorticity-velocity formulation. The transient terms added to the vorticity, energy, and species equations are presented in Eq. (9). No transient terms are added to the velocity equations:

$$\text{vorticity}: -\rho\frac{\partial \omega}{\partial t} \qquad \text{energy}: \rho c_p \frac{\partial T}{\partial t} \qquad \text{species}: \rho\frac{\partial Y_i}{\partial t} \tag{9}$$

The computer code makes use of the Portable Extensible Toolkit for Scientific Computation [34] to handle many of the difficulties of such a large and complex calculation. The libraries manage parallelization (by domain decomposition), distributed array storage, and parallel sparse matrix calculations including Krylov subspace methods, numerical Jacobian generation, preconditioners, and linear and nonlinear solvers.

F. Kinetic Mechanisms

The full AP/HTPB kinetic mechanism simulating the homogeneous binder used in this model was developed by Jeppson [31]. It consists of 44 chemical species participating in 157 reaction steps and is a modified form of the smaller AP/CTPB (carboxy-terminated polybutadiene) mechanism proposed by Korobeinichev et al. [35] with additions from Korobeinichev et al. [36], Ermolin [37], Wang et al. [38], and GRI-Mech [39]. To facilitate faster calculations, the full AP/HTPB gas-phase kinetic mechanism was analyzed for species and reactions that might be removed without changing the calculated one-dimensional burning rate. The result of this sensitivity analysis is a slightly reduced kinetic mechanism of 37 species participating in 127 reactions. The eliminated species are C, CH, CH_2CO, ClOO, H_2O_2, NNH, and NOCl. No reactions or reaction parameters were modified.

G. Verification and Validation

Numerical verification was performed based on an approach outlined by Roy [40]. Grid convergence studies were conducted for monopropellant AP combustion using the 37-species mechanism. Relative surface temperature error, as defined by Eq. (10) with $T_{s,\text{fine}} = 775.7$ K, was used for comparison. Unfortunately, an exact solution to the problem does not exist; therefore, a surface temperature predicted using a highly refined mesh was used in place of an exact value. Figure 3 presents the results of the verification study, which are consistent with the first-order upwind scheme used in the model:

$$\text{error} = \left|\frac{T_{s,\text{fine}} - T_{s,\text{current}}}{T_{s,\text{fine}}}\right| \tag{10}$$

Validation was also performed [5] comparing the numerical results with an analytical expression for diffusion through a stagnant-gas film [41], a kinetic mechanism for H_2/O_2 combustion by Kee et al. [42], and comparison to experimental data for monopropellant AP combustion [43] and homogeneous AP/HTPB combustion [44]. Modification of the model to a vorticity formulation successfully increased the stability and accuracy of the model and decreased runtime. CPU time decreased substantially, from about 1 month using the fully coupled Navier–Stokes conservation equations to around 1.5 days using the vorticity-velocity equations.

III. Results and Discussions

The vorticity formulation of the diffusion flame model has been applied to an 86%-AP/14%-HTPB propellant with 37.8% (400 μm) AP and 48.2% (12 μm) AP at 20 atm. The particle size, binder composition, and AP mass-fraction values were chosen to correspond to a propellant formulation reported by Miller and Foster [45]. It was assumed that the 12 μm AP and the HTPB formed a homogenized binder mixture. The binder thickness was varied with particle size to give an overall AP mass fraction of 0.86. The binder

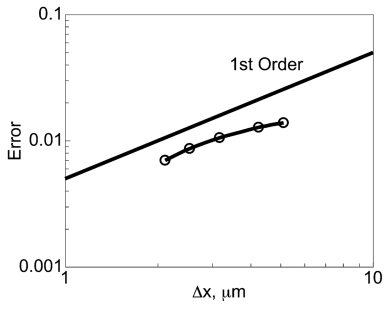

Fig. 3 Surface temperature error as a function of grid size.

thickness surrounding the AP particle was calculated based on a spherical particle of AP surrounded by a shell of homogenized binder, resulting in 89 μm of binder for the 400 μm AP particle. Taking advantage of the symmetry of the system, only half of the particle diameter was modeled. The numerical grid was 289 μm wide, corresponding to the chosen AP particle size and binder thickness, and 1300 μm long to allow the system to reach equilibrium. The minimum grid size was 0.008 μm at the propellant surface. The results presented subsequently illustrate the flame structure present above the surface of a composite propellant consisting of large AP particles.

The present model predicts the same physical picture as the BDP model with one variation: a fourth, premixed, flame is present above the homogenized binder. The fine particles of AP in the binder are assumed to be homogenized with the binder, and therefore the binder decomposition products react in the premixed fourth flame zone. The predicted flame structure for AP/HTPB combustion at 20 atm is presented in Fig. 4. The locations of the different flames, as indicated by the temperature field, are labeled. As proposed for large particles, the AP monopropellant flame, which has a final flame temperature of ~1400 K, dominates the bulk of combustion above the 400 μm AP particle. The AP monopropellant flame standoff distance is within a few microns of the surface. A primary diffusion flame is located at the interface, in which decomposition products from the binder and oxidizer mix in a very hot flame. Products from the premixed and primary diffusion flames react in a final diffusion flame, in which the adiabatic flame temperature of the system is finally reached. The final diffusion flame is too far from the surface to have any substantial impact on the burning rate. These results give further numerical support to the validity of the BDP model concepts. Comparison of Fig. 4 with the original BDP picture (Fig. 1) bares remarkable similarities.

The predicted flame structure and axial mass flux are presented in Fig. 5. The four different flame structures are distinctly present in the temperature profile. The relatively large scale of a 400 μm particle increases the radial distance across which diffusion must take place and results in the multidimensional flame structure. The proximity of the monopropellant flame above the AP particle (~8 μm) controls most of the combustion above the AP particle. The influence of the primary diffusion flame is limited to a relatively small section of the surface, and therefore the combustion of large particles is controlled by the slower AP monopropellant rate and the premixed binder rate. The final diffusion flame also appears to close over the AP particle, with lower temperatures at the outlet boundary above the binder, as would be expected for a fuel-rich diffusion flame. The axial mass flux shows a peak at the interface at which the primary diffusion flame is located, increasing the burning rate at that location. The mass flux then forms two distinct regions, one above the particle and one above

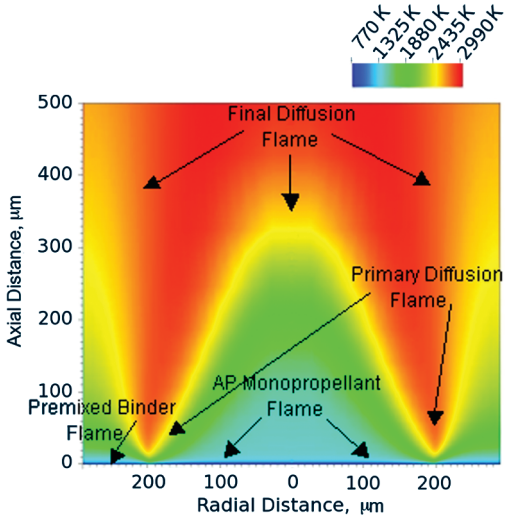

Fig. 4 Flame structure above a 400 μm particle surrounded by 89 μm of binder at 20 atm.

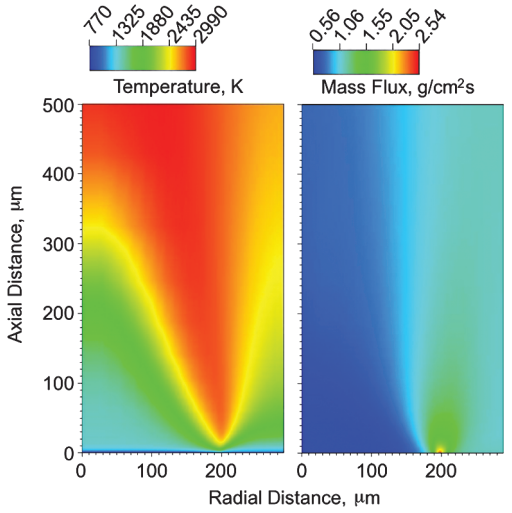

Fig. 5 Temperature and axial mass flux profiles for a 400 μm particle at 20 atm.

the binder. This is an interesting result that is common for large-particle calculations at various pressures. The exiting gases are unable to completely mix, and differing mass fluxes leave the propellant surface.

To more clearly show the details of the flame structure and examine the impact of various flames on combustion, slices of the axial temperature profile are shown in Fig. 6. Three radial positions are presented: at the AP particle center ($r = 0$ μm), at the AP/binder interface ($r = 200$ μm), and at the outer edge of the binder ($r = 289$ μm). The resultant temperature profiles give insight into the heat feedback to the surface that drives combustion and to the controlling mechanism at each location.

The temperature profile at the particle center ($r = 0$ μm) rises from the surface temperature (773 K) to approximately 1350 K within 8 μm, after which it levels off before rising again to its final temperature of nearly 3000 K, relatively far from the surface. The intermediate plateau in the centerline temperature profile corresponds to the position and temperature of the AP monopropellant flame. The final temperature of nearly 3000 K corresponds to the final diffusion flame. These trends can be seen in Fig. 7, in which the particle centerline temperature is compared with a calculated pure-AP temperature profile at 20 atm. The predicted heat flux to the surface for the composite system (1246 W/cm^2) and for the monopropellant AP (1245 W/cm^2) is essentially identical. These predictions show that the burning rate at the particle centerline is controlled by the monopropellant decomposition rate and is not impacted by the diffusion flames.

Predictions at 20 atm for the temperature profile at the radial boundary ($r = 289$ μm), above the fine AP/HTPB binder, reach 95% of the premixed binder's flame temperature (2150 K) within 80 μm of the surface. The temperature then gradually approaches the final flame temperature of the system. The temperature profile above the binder corresponds to the predicted one-dimensional

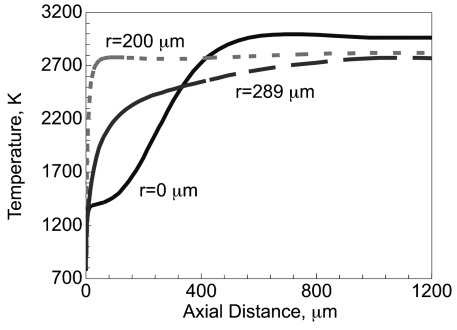

Fig. 6 Temperature profiles for a 400 μm particle at 20 atm for three radial positions: particle centerline ($r = 0$ μm), particle/binder interface ($r = 200$ μm), and radial boundary ($r = 298$ μm).

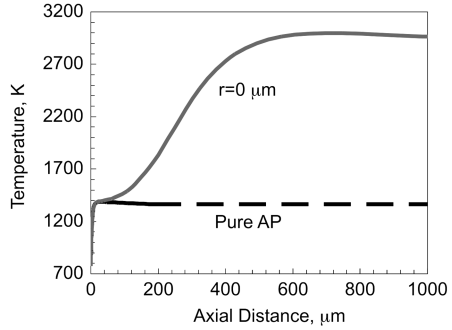

Fig. 7 Predicted temperature profiles for a 400 μm AP particle in a composite propellant at the particle centerline ($r = 0$ μm) and for pure-AP monopropellant at 20 atm.

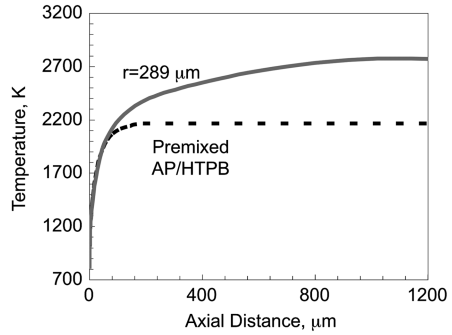

Fig. 8 Predicted temperature profiles for a 400 μm AP particle in a composite propellant above the binder ($r = 298$ μm) and the homogenized AP/HTPB monopropellant at 20 atm.

homogenized binder temperature for 77.5% AP in HTPB, as seen in Fig. 8, before rising to the final flame temperature. The predicted heat flux above the binder was 2738 W/cm^2 compared with 3024 W/cm^2 for the premixed binder alone. There is a slight impact from the diffusion flames at 20 atm, but the impact is minimal and combustion is dominated by the premixed binder flame. Because of the higher heat flux above the binder, surface regression is faster at the binder boundary than it is at the particle centerline.

The primary diffusion flame above the particle/binder interface ($r = 200$ μm) causes a much steeper temperature gradient near the surface than either the AP monopropellant flame or the premixed binder flame (see Fig. 6). The predictions show that a temperature of 2700 K is reached within approximately 35 μm of the surface: a rise of nearly 2000 K. The variation in temperature across the surface of a 400 μm particle illustrates the scale and complexity of the flame structure above a composite propellant, demonstrating why it is so difficult to obtain detailed experimental data for such a system. The heat flux above the interface is 5736 W/cm^2, roughly 2 times higher than the heat flux above the binder and 4 times higher than at the particle centerline. Therefore, the corresponding burning rate is significantly higher at the interface, compared with the rest of the surface.

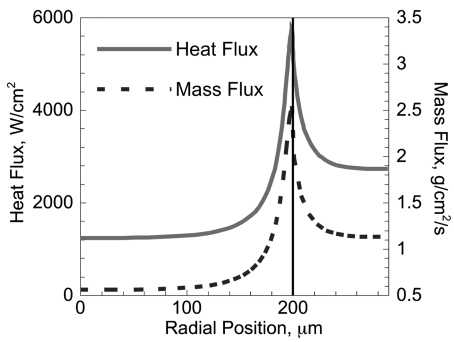

Fig. 9 Surface heat and mass flux for a 400 μm AP particle with 77.5% AP in HTPB binder at 20 atm.

The influence of the primary diffusion flame is shown graphically in Fig. 9, in which the heat flux to the surface and the corresponding mass flux are plotted as functions of radial position. The heat flux to the surface is the driving force for the decomposition and gasification of the condensed-phase materials. The mass flux at the particle/binder interface ($r = 200$ μm) is more than 4 times higher than the mass flux of the AP particle at its center ($r = 0$ μm) and more than twice the mass flux of the homogenized binder ($r = 289$ μm). This is due to the significantly higher heat feedback from the primary diffusion flame at the interface, relative to the heat flux from the AP monopropellant or binder premixed flames. The predictions indicate

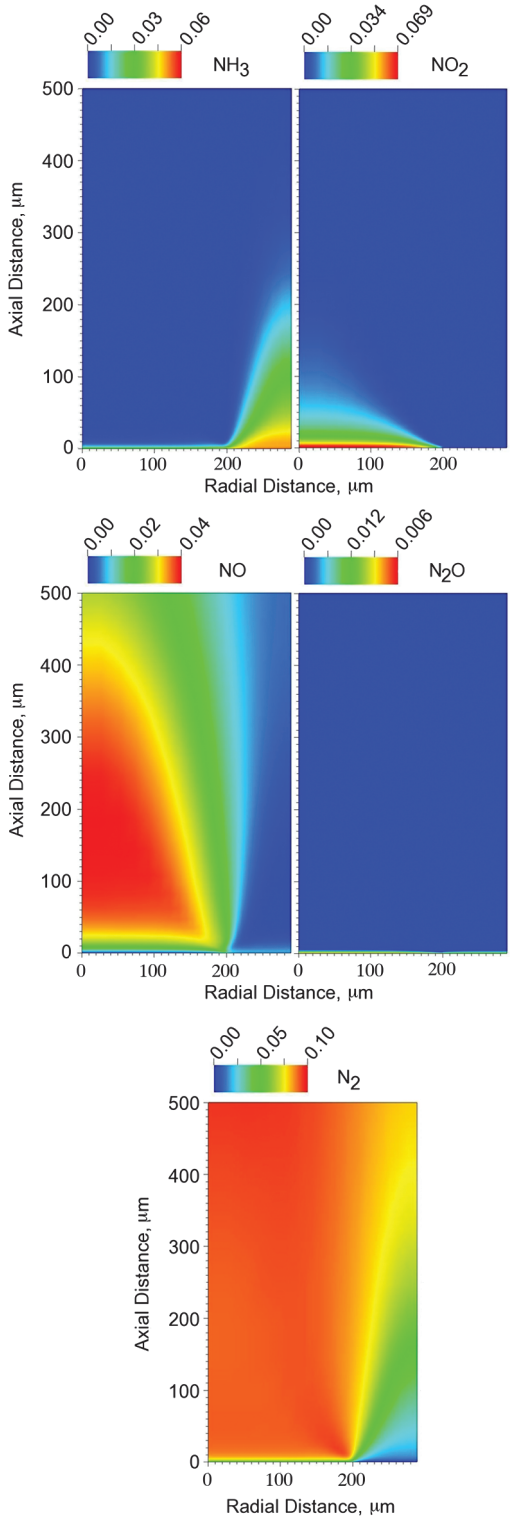

Fig. 10 Species mass fractions for the creation of N_2 from NH_3 in an oxygen-rich environment above a 400 μm AP particle at 20 atm.

that the area around the edge of the particle would be regressing much faster than the rest of the surface, creating a dynamic nonplanar burning surface. However, the surface of an actual composite propellant is expected to be much more linear, due to the changing location of the particle/binder interface as the particle burns.

The predicted regression rate is consistent with the experimental observations for sandwich-burning experiments. Korobeinichev et al. [46] and Price et al. [47] observed that the interfacial regions between laminas of AP and a binder were recessed with respect to the rest of the surface at moderate pressure. Also, note that the burning rates at both edges of the domain approach constant values, illustrating that the individual premixed flames control combustion at those locations. Examination of the mass flux above the particle shows that nearly three-fourths of the particle surface area is regressing at the AP monopropellant rate. Therefore, large-particle regression is controlled by the monopropellant rate; thus, the overall burning rate approaches the AP monopropellant limit, as expected.

These rather dramatic heat and mass flux results point out two of the limitations of the current model: the predictions are for a steady-state system and the surface is assumed to be planar. However, even with these limitations, the understanding of the flame structure that these predictions provide is significant.

Use of a detailed mechanism allows for the prediction of the flame structure without any prior assumptions, aside from the inlet species. It also allows for the prediction of species profiles. Examination of species profiles above the surface is instructive. The formation of N_2 as a final product from the destruction of NO_x species follows the general paths $NO_2 \rightarrow NO \rightarrow N_2O \rightarrow N_2$ and $NO_2 \rightarrow NO \rightarrow N_2$, where most of the NO_x species are created from the oxidation of NH_3 in the oxygen-rich environment above the AP particle. These trends are readily seen by examination of these species profiles above the surface, shown in Fig. 10.

A major decomposition product of AP is NH_3. As seen in Fig. 10, virtually all of the NH_3 is destroyed in the AP monopropellant flame within a few microns of the surface. The NH_3 released from the AP in the binder is not readily consumed due to the lack of oxygen in that region. Further, the NH_3 released above the binder undergoes a decomposition path that does not include NO_2 as an intermediate. This is due to the fuel-rich nature of that region. The destruction of NH_3 above the AP particle leads to the formation of NO_2. As the concentration of NH_3 drops, the concentration of NO_2 rises. The destruction of NO_2 leads to the formation of NO, which has a longer residence time, as noted by its presence 500 μm from the surface. NO is then either converted to N_2O or directly to N_2. The conversion of N_2O to N_2 is apparently very rapid, as noted by the essentially zero mass fraction of N_2O in the entire domain. Examination of Fig. 10 shows that as NO is destroyed, the amount of N_2 increases above the particle. It can also be seen that the lack of oxygen above the binder results in much slower production of N_2, and the equilibrium mass fraction of N_2 above the binder is not achieved within the calculated grid.

The mixture of AP/HTPB in the binder results in much of the NH_3 from the AP being quickly converted to HCN. The lack of oxygen creates an alternative path in which NH_3 is converted to N_2 by $NH_3 \rightarrow NH \rightarrow N_2$. The HCN is slowly converted to N_2, as seen in Fig. 11.

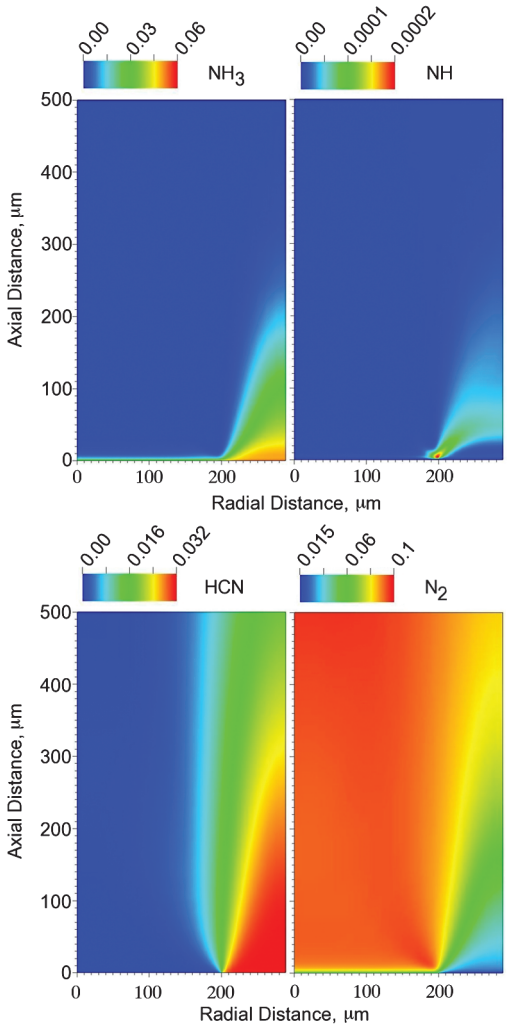

Fig. 11 Species mass fractions for the production of N_2 in the fuel-rich region above the binder for a 400 μm AP particle at 20 atm.

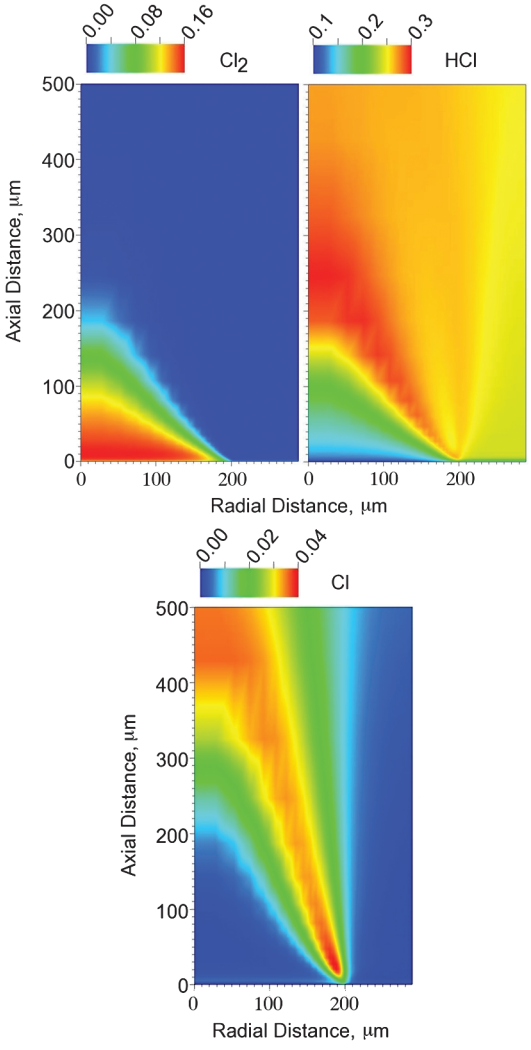

Fig. 12 Species mass fractions for Cl_2, HCl, and Cl above a 400 μm AP particle surrounded by binder.

Another decomposition path of interest is the formation of HCl and Cl. The path generally follows $Cl_2 \rightarrow HCl \rightarrow Cl$ and can be seen in Fig. 12. Large amounts of Cl_2 are generated by the monopropellant flame above the AP particle. This is then converted into HCl. Then, when large concentrations of HCl are present at high temperatures, the radical Cl is created in small amounts.

Comparison of the O_2 concentration to some of the major final species is presented in Fig. 13. When O_2 exists in large concentrations, above the AP particle, many of the final species are absent, particularly carbon-containing species. Oxygen and carbon must diffuse together before those species are created. Large amounts of CO_2 exit the primary diffusion flame, in which oxygen is in abundance, but as CO_2 interacts with the fuel-rich products, oxygen is transferred from CO_2, creating CO. Also, the lack of oxygen results in large amounts of H_2 being created in the fuel-rich region of the flame as the carbon is converted to CO.

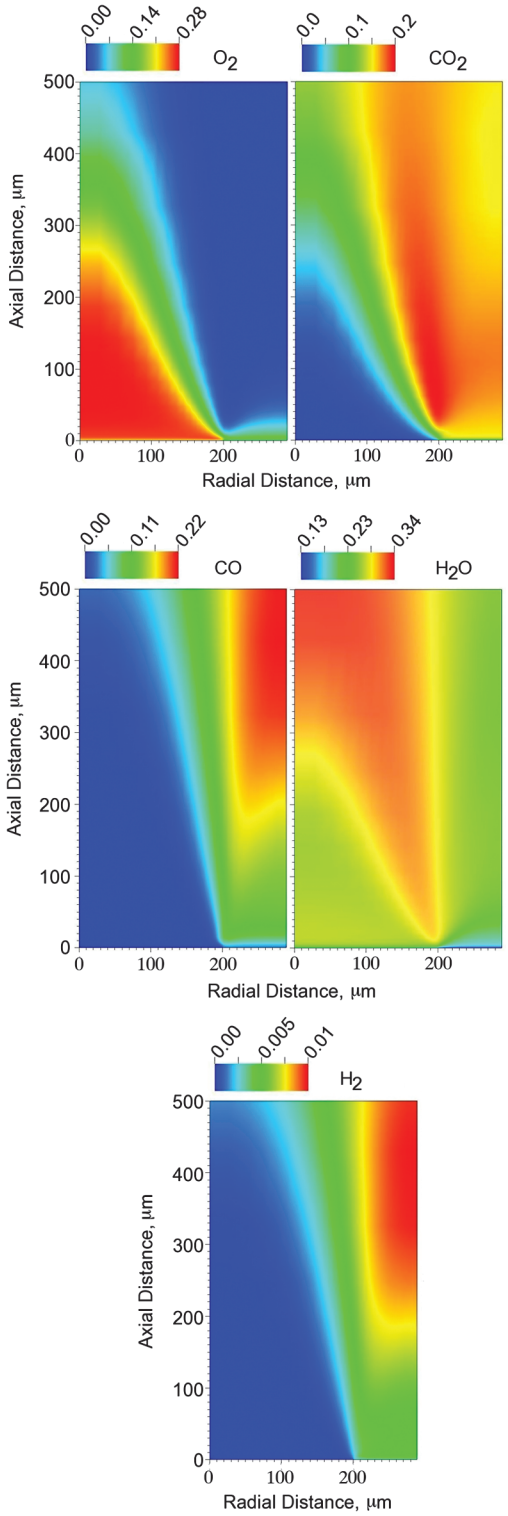

Fig. 13 Conversion of O_2 to final species above a 400 μm AP particle at 20 atm.

IV. Conclusions

A two-dimensional model has been developed to simulate the complex flame structure above an idealized AP/HTPB composite propellant using a vorticity-velocity formulation of the conservation equations. A detailed gas-phase kinetic mechanism with 37 chemical species and 127 reaction steps is employed to describe the reactions involved. Inlet conditions to the gas phase are derived from one-dimensional-model calculations. The inlet conditions along with the kinetic mechanism and species diffusion are allowed to determine the flame structure of the system.

The model was applied to an 86%-AP/14%-HTPB propellant with 37.8% (400 μm) AP and 48.2% (12 μm) AP. It is assumed that the 12 μm AP and the binder make up a homogenized binder mixture that can be modeled as a premixed flame. The predicted results show the detailed diffusion flame structure above the idealized composite propellant surface, and results are qualitatively consistent with the BDP model. The AP monopropellant flame, the primary diffusion flame, and the final diffusion flame are all apparent in the prediction, along with a premixed flame over the binder. The dominant contribution of the primary diffusion flame to the propellant's burning rate is shown. The predictions show that the heat flux at the AP/binder interface is approximately 4 times that at the AP center and 2 times that above the binder, emphasizing the importance of the primary diffusion flame. Use of the detailed kinetic mechanism also allows one to follow the species concentrations of various reaction intermediates, thus providing better understanding the chemistry of the flames.

Acknowledgments

This work was funded by a subcontract from Software and Engineering Associates, Carson City, Nevada, which was funded by Office of Naval Research contract N00014-02-C-0292, with Judah Goldwasser as contract monitor.

References

[1] Felt, S. A., and Beckstead, M. W., "A Model of the AP/HTPB Diffusion Flame," *Proceedings of the 39th JANNAF Combustion Subcommittee Meeting*, JSC CD-24, Chemical Propulsion Information Agency, Columbia, MD, 2003.

[2] Felt, S. A., "Two-Dimensional Modeling of AP Composite Propellant Flame Structure with Detailed Kinetics," Ph.D. Dissertation, Department of Chemical Engineering, Brigham Young Univ., Provo, UT, 2004.

[3] Gross, M. L., Felt, S. A., and Beckstead, M. W., "Two-Dimensional Modeling of AP Composite Propellants with Detailed Kinetics: Effects of Particle Size and Pressure," AIAA Paper 2006-4925, July 2006.

[4] Gross, M. L., and Beckstead, M. W., "Pressure Effects on the AP/HTPB Diffusion Flame," *Proceedings of the 41st JANNAF Combustion Subcommittee Meeting*, JSC CD-46, Chemical Propulsion Information Agency, Columbia, MD, Dec. 2006.

[5] Gross, M. L., "Two-Dimensional Modeling of AP/HTPB Utilizing a Vorticity Formulation and One-Dimensional Modeling of AP and ADN," Ph. D. Dissertation, Dept. of Chemical Engineering, Brigham Young Univ., Provo, UT, 2007.

[6] Beckstead, M. W., Derr, R. L., and Price, C. F., "A Model of Composite Solid-Propellant Combustion Based on Multiple Flames," *AIAA Journal*, Vol. 8, No. 12, Dec. 1970, pp. 2200–2207. doi:10.2514/3.6087

[7] Beckstead, M. W., "Combustion Calculations for Composite Solid Propellants," *Proceedings of the 13th JANNAF Combustion Subcommittee Meeting*, 281, Vol. 2, Chemical Propulsion Information Agency, Columbia, MD, 1976, pp. 299–312.

[8] Smooke, M. D., Yetter, R. A., Parr, T. P., and Hanson-Parr, D. M., "Experimental and Modeling Studies of Two-Dimensional Ammonium Perchlorate Diffusion Flames," *Proceedings of the Combustion Institute*, Vol. 28, No. 1, 2000, pp. 839–846.

[9] Cai, W., and Yang, V. A., "Model of AP/HTPB Composite Propellant Combustion," AIAA Paper 2000-0311, 2000.
[10] Davis, I. L., and Carter, R. G., "Random Particle Packing by Reduced Dimension Algorithms," *Journal of Applied Physics*, Vol. 67, No. 2, 1990, pp. 1022–1029. doi:10.1063/1.345785
[11] Webb, M. D., and Davis, I. L., "Random Particle Packing with Large Particle Size Variations Using Reduced-Dimension Algorithms," *Powder Technology*, Vol. 167, No. 1, 2006, pp. 10–19. doi:10.1016/j.powtec.2006.06.003
[12] Sankaralingam, K., and Chakravarthy, S. R., "A Computer Model of Flamelet Distribution on the Burning Surface of a Composite Solid Propellant," *Combustion Science and Technology*, Vol. 161, Nos. 1–6, 2000, pp. 49–68. doi:10.1080/00102200008935811
[13] Knott, G. M., Jackson, T. L., and Buckmaster, J., "Random Packing of Heterogeneous Propellants," *AIAA Journal*, Vol. 39, No. 4, Apr. 2001, pp. 678–686. doi:10.2514/2.1361
[14] Kochevets, S., Buckmaster, J., Jackson, T. L., and Hegab, A., "Random Packs and Their Use in the Modeling of Heterogeneous Solid Propellant Combustion," *Journal of Propulsion and Power*, Vol. 17, No. 4, July–Aug. 2001, pp. 883–891. doi:10.2514/2.5820
[15] Wang, X., Buckmaster, J., and Jackson, T. L., "Burning of Ammonium-Perchlorate Ellipses and Spheroids in Fuel Binder," *Journal of Propulsion and Power*, Vol. 22, No. 4, July–Aug. 2006, pp. 764–768. doi:10.2514/1.15739
[16] Matous, K., Inglis, H. M., Gu, X., Rypl, D., Jackson, T. L., and Geubelle, P. H., "Multiscale Modeling of Solid Propellants: From Particle Packing to Failure," *Composites Science and Technology*, Vol. 67, Nos. 7–8, June 2007, pp. 1694–1708. doi:10.1016/j.compscitech.2006.06.017
[17] Massa, L., Jackson, T. L., Buckmaster, J., and Campbell, M., "Three-Dimensional Heterogeneous Propellant Combustion," *Proceedings of the Combustion Institute*, Vol. 29, No. 2, 2002, pp. 2975–2983. doi:10.1016/S1540-7489(02)80363-7
[18] Massa, L., Jackson, T. L., and Buckmaster, J., "New Kinetics for a Model of Heterogeneous Propellant Combustion," *Journal of Propulsion and Power*, Vol. 21, No. 5, Sept.–Oct. 2005, pp. 914–924. doi:10.2514/1.2433
[19] Parr, T. P., Hanson-Parr, D. M., Smooke, M. D., and Yetter, R. A., "Ammonium Perchlorate/(H2 + CO) Gaseous Fuel Diffusion Flame Studies," *Proceedings of the Combustion Institute*, Vol. 29, No. 2, 2002, pp. 2881–2888. doi:10.1016/S1540-7489(02)80352-2
[20] Parr, T. P., Hanson-Parr, D. M., Smooke, M. D., and Yetter, R. A., "AP/(N2 + C2H2 + C2H4) Gaseous Fuel Diffusion Flame Studies," *Proceedings of the Combustion Institute*, Vol. 30, No. 2, 2005, pp. 2113–2121. doi:10.1016/j.proci.2004.08.108
[21] Kee, R. J., Coltrin, M. E., and Glarborg, P., *Chemically Reacting Flow: Theory & Practice*, Wiley, Hoboken, NJ, 2003.
[22] Keshtiban, I. J., Belblidia, F., and Webster, M. F., "Compressible Flow Solvers for Low Mach Number Flows—A Review," Inst. of Non-Newtonian Fluid Mechanics, Univ. of Wales, Swansea, Wales, U.K., http://www.cs.swan.ac.uk/reports/yr2004/CSR2-2004.pdf [retrieved Apr. 2007].
[23] Oran, E. S., and Boris, J. P., *Numerical Simulation of Reactive Flow*, Cambridge Univ. Press, Cambridge, England, U.K., 2001.
[24] Patankar, S. V., *Numerical Heat Transfer and Fluid Flow*, Taylor & Francis, Bristol, PA, 1980.
[25] Massa, L., Jackson, T. L., and Short, M., "Numerical Solution of Three-Dimensional Heterogeneous Solid Propellants," *Combustion Theory and Modeling*, Vol. 7, No. 3, Sept. 2003, pp. 579–602. doi:10.1088/1364-7830/7/3/308
[26] Smooke, M. D., Mitchell, R. E., and Keyes, D. E., "Numerical Solution of Two-Dimensional Axisymmetric Laminar Diffusion Flames," *Combustion Science and Technology*, Vol. 67, Nos. 4–6, 1989, pp. 85–122. doi:10.1080/00102208908924063
[27] Bennett, B. A. V., and Smooke, M. D., "Local Rectangular Refinement with Application to Axisymmetric Laminar Flames," *Combustion Theory and Modeling*, Vol. 2, No. 3, 1998, pp. 221–258. doi:10.1088/1364-7830/2/3/001
[28] Dworkin, S. B., Bennett, B. A. V., and Smooke, M. D., "A Mass-Conserving Vorticity-Velocity Formulation with Application to Nonreacting and Reacting Flows," *Journal of Computational Physics*, Vol. 215, No. 2, 2006, pp. 430–447. doi:10.1016/j.jcp.2005.11.002
[29] Kuo, K. K., *Principles of Combustion*, Wiley, Hoboken, NJ, 2005.
[30] Jing, Q., Beckstead, M. W., and Jeppson, M., "Influence of AP Solid Phase Decomposition on Temperature Profile and Sensitivity," AIAA Paper 98-0448, 1998.
[31] Jeppson, M. B., "A Kinetic Model for the Premixed Combustion of a Fine AP/HTPB Composite Propellant," M.S. Thesis, Brigham Young Univ., Provo, UT, 1998.
[32] Kee, R. J., Dixon-Lewis, D., Warnatz, J., Coltrin, M. E., and Miller, J. A., "A Fortran Computer Code Package for the Evaluation of Gas-Phase Multicomponent Transport Properties," Sandia National Labs., Rept. SAND86-8246, Albuquerque, NM, 1992.
[33] Kee, R. J., Rupley, F. M., and Miller, J. A., "CHEMKIN-II: A FORTRAN Chemical Kinetics Package for the Analysis of Gas-Phase Chemical Kinetics," Sandia National Labs., Rept. SAND89-8009B, Albuquerque, NM, 1991.
[34] *Portable, Extensible Toolkit for Scientific Computation* [online database], http://www.mcs.anl.gov/petsc/ [retrieved Jan. 2006].
[35] Korobeinichev, O. P., Ermolin, N. E., Chernov, A. A., and Emel'yanov, I. D., "Flame Structure, Kinetics and Mechanism of Chemical Reactions in Flames of Mixed Composition Based on Ammonium Perchlorate and Polybutadiene Rubber," *Combustion, Explosion, and Shock Waves*, Vol. 28, No. 4, July–Aug. 1992, pp. 366–371. doi:10.1007/BF00789954
[36] Korobeinichev, O. P., Chernov, A. A., Emel'yanov, I. D., Ermolin, N. E., and Trofimycheva, T. V., "Investigation of the Kinetics and the Chemical Reaction Mechanism in the Flame of a Mixed Compound, Based on Ammonium Perchlorate and Polybutadiene Rubber," *Combustion, Explosion, and Shock Waves*, Vol. 26, No. 3, Nov. 1990, pp. 292–300. doi:10.1007/BF00751367
[37] Ermolin, N. E., "Model for Chemical Reaction Kinetics in Perchloric Acid-Ammonia Flames," *Combustion, Explosion, and Shock Waves*, Vol. 31, No. 5, 1995, pp. 555–565. doi:10.1007/BF00743807
[38] Wang, H., Sung, C. J., and Law, C. K., "On Mild and Vigorous Oxidation of Mixtures of Chlorinated Hydrocarbons in Droplet Burning," *Combustion and Flame*, Vol. 110, No. 1, July 1997, pp. 222–238. doi:10.1016/S0010-2180(97)00066-7
[39] *GRI-Mech 3.0* [online database], http://www.me.berkeley.edu/gri_mech/ [retrieved 1998].
[40] Roy, C. J., "Review of Code and Solution Verification Procedures for Computational Simulation," *Journal of Computational Physics*, Vol. 205, No. 1, 2005, pp. 131–156. doi:10.1016/j.jcp.2004.10.036
[41] Bird, R., Stewart, W., and Lightfoot, E., *Transport Phenomena*, Wiley, New York, 2002.
[42] Kee, R. J., Grcar, J. F., Smooke, M. D., and Miller, J. A., "A Fortran Program for Modeling Steady Laminar One-Dimensional Premixed Flames," Sandia National Labs., Rept. SAND85-8240, Albuquerque, NM, 1992.
[43] Atwood, A. I., Boggs, T. L., Curran, P. O., Parr, T. P., Hanson-Parr, D. M., Price, C. F., and Wiknich, J., "Burning Rate of Solid Propellant Ingredients, Part 1: Pressure and Initial Temperature Effects," *Journal of Propulsion and Power*, Vol. 15, No. 6, Nov.–Dec. 1999, pp. 740–747. doi:10.2514/2.5522
[44] Foster, R. L., Condon, J. A., and Miller, R. R., "Low Exponent Technology," U.S. Air Force Rocket Propulsion Lab., Rept. TR-81-95, Edwards AFB, CA, 1982.
[45] Miller, R. R., and Foster, R. L., "The Influence of the Fine AP/Binder Matrix on Composite Propellant Ballistic Properties," *Proceedings of the 17th JANNAF Combustion Subcommittee Meeting*, 329, Vol. 3, Chemical Propulsion Information Agency, Columbia, MD, 1980, pp. 91–104.
[46] Korobeinichev, O. P., Tereschenko, A. G., Shvartsberg, V. M., Chernov, A. A., Makhov, G. A., and Zabolotny, A. E., "A Study of Flame Structure of Sandwich Systems Based on Ammonium Perchlorate, HMX, and Polybutadiene Binder," *Flame Structure*, Vol. 1, 1991, pp. 262–267.
[47] Price, E. W., Handley, J. C., Panyam, R. R., Sigman, R. K., and Ghosh, A., "Combustion of Ammonium Perchlorate-Polymer Sandwiches," *AIAA Journal*, Vol. 19, No. 3, 1981, pp. 380–386. doi:10.2514/3.7775

S. Son
Associate Editor